Published in final edited form as:

ACS Infect Dis. 2016 October 14; 2(10): 702–713. doi:10.1021/acsinfecdis.6b00095.

Structure-function profile of MmpL3, the essential mycolic acid transporter from *Mycobacterium tuberculosis*

Juan Manuel Belardinelli[#1,~], **Amira Yazidi**[#2,3,~], **Liang Yang**[4], **Lucien Fabre**[3,5], **Wei Li**[1], **Benoit Jacques**[2], **Shiva kumar Angala**[1], **Isabelle Rouiller**[3,5], **Helen I. Zgurskaya**[4,#], **Jurgen Sygusch**[2,3,#], and **Mary Jackson**[1,#]

[1]Mycobacteria Research Laboratories, Department of Microbiology, Immunology and Pathology, Colorado State University, Fort Collins, CO 80523-1682, USA

[2]Biochimie et Médecine Moléculaire, Université de Montréal, CP 6128, Station Centre-Ville, Montréal, Quebec, H3C 3J7, Canada

[3]Groupe d'Étude des Protéines Membranaires (GÉPROM), Université de Montréal, CP 6128, Station Centre-Ville, Montréal, Quebec, H3C 3J7, Canada

[4]University of Oklahoma, Department of Chemistry and Biochemistry, 101 Stephenson Parkway, Norman, OK 73019, USA

[5]Department of Anatomy and Cell Biology, McGill University, 3640 University Street, Montréal, Quebec, H3A 2B2, Canada

[#] These authors contributed equally to this work.

Abstract

The MmpL family of proteins translocates complex (glyco)lipids and siderophores across the cell envelope of mycobacteria and closely related *Corynebacteriaceae*, and plays important roles in the biogenesis of the outer membrane of these organisms. Despite their significance in the physiology and virulence of *Mycobacterium tuberculosis*, and from the perspective of developing novel antituberculosis agents, little is known about their structure and mechanism of translocation. In this study, the essential mycobacterial mycolic acid transporter, MmpL3, and its ortholog in *Corynebacterium glutamicum*, CmpL1, were investigated as prototypical MmpL proteins to gain insight into the transmembrane topology, tertiary and quaternary structures, and functional regions of this transporter family. Our combined genetic, biochemical and biophysical studies indicate that MmpL3 and CmpL1 are structurally similar to Gram-negative Resistance-Nodulation and Division efflux pumps. They harbor twelve transmembrane segments interrupted by two large soluble

To whom correspondence should be addressed: Mary.Jackson@colostate.edu; elenaz@ou.edu; jurgen.sygusch@umontreal.ca.
[#]co-senior authors
[~]co-first authors

SUPPORTING INFORMATION

Detailed experimental procedures and additional references, and analytical data.

AUTHOR CONTRIBUTIONS

HZ, IR, JS and MJ designed the study. JMB, LY, WL generated mutated variants of MmpL3 and performed FM-labeling and functional studies. JMB generated and analyzed the *tmaT* knock-down mutant. SKA analyzed lipids. LZ and AY performed the gel filtration studies. AY together with JS generated the CmpL1 and MmpL3 models. AY and LF conducted the negative staining EM. HZ, IR, JS and MJ wrote the manuscript with comments from all authors.

periplasmic domains, and function as homotrimers to export long-chain (C_{22}-C_{90}) mycolic acids, possibly in their acetylated form, esterified to trehalose. The mapping of a number of functional residues within the middle region of the transmembrane domain of MmpL3 shows a striking overlap with mutations associated with resistance to MmpL3 inhibitors. Our results suggest that structurally diverse inhibitors of MmpL3 all target the proton translocation path of the transporter and that multi-resistance to these inhibitors is enabled by conformational changes in MmpL3.

Graphical abstract

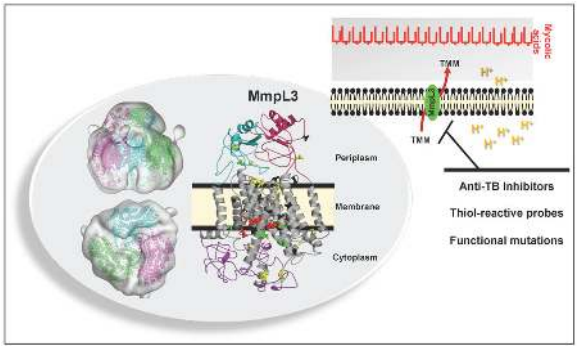

Keywords

Mycobacterium; tuberculosis; MmpL3; acyltrehaloses; mycolic acids; lipid translocation

In recent years, the MmpL (*m*ycobacterial *m*embrane *p*roteins, *l*arge) proteins have emerged as critical players in the building of the cell envelope of mycobacteria and closely related *Corynebacteriaceae*. The MmpL family of proteins is a subset of the Resistance, Nodulation, and Division (RND) superfamily of transporters which, in bacteria, archaea and eukaryotes, mediate the proton-dependent export of substrates. Accordingly, they share with other RND transporters a requirement for the electrochemical proton gradient across the inner membrane for activity as well as predicted conserved topological features.[1-7] More than twenty years of genetic and biochemical studies, combined with the availability of multiple crystal structures and computational modeling, have allowed the fundamentals of the mechanisms of action, substrate specificity and energetics of prototypical Gram-negative RND transporters such as the major multidrug efflux pump AcrB of *E. coli* to be relatively well characterized.[8-10]

The genome of *Mycobacterium tuberculosis* (*Mtb*) encodes 13 MmpL proteins, the functions of seven of which have been at least partially established. In comparison, the genome of *Corynebacterium glutamicum* (*Cgl*) encodes only 4 MmpL-like proteins, referred to as CmpLs. Unlike AcrB-type multidrug efflux pumps, the MmpL/CmpL proteins of *Corynebacteriaceae* appear to export endogenous lipophilic molecules rather than exogenous ones, and to display a relatively narrow substrate specificity.[3-4,11-15] Other than impacting the composition of the mycobacterial cell envelope and thus, indirectly, its permeability to biocides, the MmpL proteins of *Mtb* do not seem to play an active role in drug resistance, exception made of MmpL5 that participates in the active efflux of clofazimine, bedaquiline

and azole drugs.[4,16-21] A decade of functional studies indicate that MmpL proteins have specialized in the translocation of physiologically essential and/or biologically active secreted and outer membrane (OM) constituents, including (glyco)lipids and siderophores.[3-4,11-15,22] On the basis of their heme-binding properties *in vitro*, two MmpL proteins, MmpL3 and MmpL11, were further proposed to be involved in a heme-iron acquisition system.[23-24] The structure of one of the two soluble periplasmic domains of MmpL11 was solved [6], a transport mechanism based on dynamics simulation was proposed for MmpL5 [25] and the use of prediction algorithms yielded different topological models for MmpL3 and other MmpL proteins. [5-7,11,13,26] Yet, despite their significance in the physiology and virulence of *Mtb*, and from the perspective of anti-TB drug development,[5,26-35] no full-size MmpL protein has yet been purified and reconstituted *in vitro*. As a result, the transmembrane topology of no MmpL protein had yet been validated experimentally and even basic biochemical properties of these proteins, such as their oligomeric state, determinants of substrate specificity, mechanism of translocation and putative physical association with other inner membrane, periplasmic and/or OM proteins remain to a large extent unknown. In the studies described herein, the essential trehalose monomycolate (TMM) transporter, MmpL3, and its ortholog in *Cgl*, CmpL1 (Ncgl2769), were used as prototypes to gain insight into functional aspects of MmpL transporters, and lay the mechanistic and structural foundations required for the future rational development of novel anti-TB therapeutics targeting this family of transporters.

RESULTS AND DISCUSSION

Quarternary structure of MmpL3 and CmpL1

A characteristic mechanistic feature of the archetypal AcrB transporter from *E. coli* and MexB transporter from *Pseudomonas aeruginosa* is that these proteins function as obligatory homotrimers.[8,10] To determine whether MmpL or CmpLs proteins form oligomers, we chose MmpL3 and its corynebacterial ortholog, CmpL1 (Ncgl2769; 42% identity; 62% similarity to MmpL3 on a 765 amino acid overlap). Both proteins serve an essential function in the translocation of long-chain (C_{22}-C_{38} in *Corynebacterium*; C_{60}-C_{90} in *Mycobacterium*) α-branched, β-hydroxylated fatty acids known as mycolic acids, which are major constituents of the inner and outer leaflets of the OM of *Corynebacteriaceae*. Importantly, MmpL3 is thought to be the target of a number of anti-TB inhibitors under development.[5,26-35] MmpL3 (MW = 101 kDa) and CmpL1 (MW = 83 kDa) which we purified from *Cgl* cells were treated with the amine reactive cross-linker dithiobis(succinimidylpropionate) and the cross-linked proteins were analyzed by immunoblotting. High molecular weight species (~ 300 kDa) became apparent with increasing concentrations of the cross-linker suggestive of protein oligomerization or formation of stable complexes. Based on electrophoretic mobilities, both cross-linked protein samples contained dimeric and trimeric forms that were sensitive to the addition of the reducing agent dithiothreitol [Fig. S1a and data not shown]. Thus, both MmpL3 and CmpL1 are prone to oligomerization. Further size exclusion chromatography analyses indicated that purified CmpL1 is homogeneous and yields a single peak with a molecular weight ~ 315 kDa [Fig. S1 a-b] for the protein-detergent complex, which is consistent with a trimeric quaternary structure surrounded by a DDM detergent corona of 65 kDa.

Low resolution structure of CmpL1

We next turned to single particle electron microscopy (EM) to delineate the molecular envelope of CmpL1. Observations of CmpL1 by negative staining revealed a homogeneous distribution of particles ~ 100Å in diameter in various orientations on the EM grid [Fig. 1a]. The map shown was calculated from 6,701 particles enforcing a C3 symmetry. The autorefine routine stopped at the angular sampling of 3.5 degrees. 2D analysis as well as a probabilistic initial 3D model confirmed a trimeric symmetric shape (C3 symmetry) of the particles [Fig. 1 b-c]. Refinement of this model imposing C3 symmetry led to the 18Å resolution EM map shown in Fig. 2.

A model for the 3D structure of CmpL1 was prepared based on its primary amino acid sequence and two top structural homologs, SecDF from *Thermus thermophiles* and *E. coli* AcrB, using the I-TASSER server [Table S1].[36] The modeled structure and its fit to the EM envelope are shown in Figure 2 and as a movie [movie S1]. Although several other *ab initio* models were built of CmpL1 using the I-TASSER or Phyre2 servers and all models had similar folds of the transmembrane helices, our current model had the advantage of being able to fit into the low resolution EM map by simple rigid body displacements of its periplasmic domains. The EM envelope exhibited a deep central vestibule with three distinct channels and crevasses that afforded facile orientation of the CmpL1 structural model. The clear demarcation between each subunit in the EM envelope is consistent with an organization of the transmembrane domain as clusters of helices and was exploited to reposition the orientations of the two periplasmic domains [thereafter referred to as PN (residues 34-173) and PC (residues 392-511) by analogy to the terminology used for AcrB], the overall tilt of the transmembrane domain and the disposition of the C-terminal region (residues 688-772). The fit of the modeled CmpL1 trimer to the EM envelope was further improved by real space refinement that yielded good metrics shown in Table 1.

CmpL1 and MmpL3 structural features

The refined structure for CmpL1 was then used for template-based modeling of the MmpL3 sequence using I-TASSER and further refined as detailed in the Supporting Methods yielding an initial structural model for the MmpL3 protomer [Fig. 3a] and, consequently, of its trimeric quaternary structure [Fig. S2]. The two structures are similar and share several conserved features. By analogy with AcrB, the trimeric CmpL1/MmpL3 could be divided into three domains: the periplasmic “porter” domain, the transmembrane proton translocation domain and the C-terminal cytoplasmic domain. The transmembrane domains in each subunit of the refined CmpL1/MmpL3 structure are topologically similar to AcrB and positioned in a region of density in the EM map that forms a continuous belt of density surrounding the CmpL1 trimer, consistent with the expected position of the DDM detergent corona. As in the AcrB structure, TMS-1 of one protomer faces TMS-8 of the neighboring protomer to encircle a central vestibule. TMS-4 and TMS-10 of CmpL1/MmpL3, which contain highly conserved acidic and basic residues [Fig. S3], form the core of each transmembrane alpha-helical bundle [Fig. 2]. In AcrB, the corresponding charged residues located in TMS-4 and TMS-10, which may be protonated or deprotonated, are essential for activity [Fig. 3b and 3c]; they appear to be critical not only for proton uptake but also to function as a conformational electrostatic switch that empowers the periplasmic domain to

expel substrates.[10] The three-fold repeated channels, seen in Fig. 2a, are situated on the outer leaflet of the plasma membrane. The central vestibule of the CmpL1/MmpL3 structure is accessible both from the cytoplasm and from the periplasmic channels [Fig. 2a]. Although the vestibule interior is lined by hydrophobic residues, it may not be filled by lipids, as it is accessible to negative staining. The large separation between the transmembrane regions of the subunits forms an extensive crevasse and suggests that MmpL3/CmpL1 proteins may be able to capture their TMM substrate from the lipid bilayer as well as from the cytoplasm and sequester it into the vestibule.

The porter domain in MmpL3 is formed by residues L34 through L173 (PN) and L417 through S551 (PC) [Fig. 3a]. In AcrB, this domain interfaces with the periplasmic subunit AcrA and contains the substrate-binding pocket accessible from the periplasm and the cytoplasmic membrane.[8-10] The periplasmic PN porter domain in each MmpL3 subunit forms an interaction surface with its counterpart in the adjacent protomer that promotes the formation of the quaternary structure [Fig. S2]. The reorientation of the PN and PC porter domains in order to fill the density in the EM envelope resulted in the formation of a central pore bounded by the PN and PC domains and the periplasmic region of TMS-4 and 10, that can be seen as a hole in the EM map at high contour levels and as a dimple at lower contour levels [Fig. 2a]. MmpL3/CmpL1 lacks the TolC-docking domain of AcrB needed for the recruitment of the OM channel TolC. The C-terminal region appears to form a compact structure that interacts with the cytoplasmic side of the TM helices and is unique to CmpL1, MmpL3 and a few other HAE-2 family RND transporters [Fig. 2a; Fig. 3a; Fig. S2].[1]

The modeled structures of the MmpL3 PN and PC periplasmic regions were structurally similar and superimposed with an RMS = 3.05Å, while the structure of the equivalent MmpL11 PC fragment (PDB ID: 4Y0L),[6] homologous to the MmpL3 PC region, displayed the same topological fold as those predicted for the PN and PC regions of our model. The helical axis of TMS-11 is approximately parallel to the 3-fold axis of the MmpL3 trimer [Fig. 3a] and has a length of 33Å based on Cα carbons. This length is similar to that of TMS that span the transmembrane region in AcrB and SecDF. The estimated heights of the periplasmic and cytoplasmic regions of MmpL3 are 35Å and 25Å, respectively, when defined as cross-sections perpendicular to the 3-fold axis in the MmpL3 model [Fig. 2 and Fig. 3a].

Model validation

The main approach used here to experimentally validate the topology of MmpL3 in intact cells has consisted of introducing cysteine residues into a recombinant MmpL3 protein expressed in *Cgl* and determining their accessibility to the fluorescent thiol-reactive probe, fluorescein-5-maleimide (FM). FM has been reported to permeate both the outer and inner membranes and to label Cys residues exposed to an aqueous solution but not embedded in a membrane.[37] *Cgl* was chosen as an expression system for these experiments as it possesses a cell envelope structurally and functionally similar to that of mycobacteria and prior attempts to express *mmpL3* in *E. coli* and *Mycobacterium smegmatis* (*Msmg*) resulted in lower production yields. Because MmpL3 contains four intrinsic Cys (C24; C216; C332; and C730), we first constructed by site-directed mutagenesis a triple cysteine MmpL3 mutant

(ΔCys-MmpL3) in which C24, C332 and C730 were replaced by serine residues. When expressed in *Cgl*, ΔCys-MmpL3 did not react with FM indicating that the remaining C216 residue of MmpL3, most likely due to its localization in TMS-3, may not need to be mutated since it does not generate any background signal [Fig. 4a]. Importantly, the ability of Δ*Cys-mmpL3* expressed from the mycobacterial expression plasmid pMVGH1 to rescue the growth of an *mmpL3* null mutant of *Msmg* indicated that this variant had retained an active conformation (see functional studies further in the text). Cys residues were introduced at 30 different positions of the predicted transmembrane domains of ΔCys-MmpL3 and in the loops bracketing these domains [Fig. S3], and the resulting mutants were produced as Strep-tagged proteins in the *Cgl* strain LY108.[4] Upon labeling of the recombinant strains with the fluorescent probe FM, the ΔCys-MmpL3 variants were purified to confirm expression [Fig. S3a] and determine their labeling status [Fig. 4b]. All six extracellular loops were confirmed by labeling at least one Cys residue located in the predicted loop [Fig. 3a; Fig. S3b]. The periplasmic localization of the two large soluble loops (PN and PC) and cytoplasmic localization of the C-terminus of MmpL3 in their natural mycobacterial environment was further confirmed by expressing three MmpL3-GFP fusions, one in each of the two large soluble loops and one at the C-terminal end of the *Msmg* MmpL3 protein, in *Msmg* using the reporter plasmids pJB(−) and JB(+) [Fig. 4c; Fig. S3b].[14] Altogether, our topology studies thus support the MmpL3 model shown in Fig. 3.

Identification of functional residues in MmpL3

To identify potential functional residues in MmpL3, sequence alignments of the entire MmpL3 protein were first conducted against the NCBI database, Gram-negative and Gram-positive RND transporters, and the mycolyltransferases encoded by *fbpA*, *fbpB* and *fbpC* with which MmpL3 is expected to share the ability to bind trehalose and/or mycolic acyl chains. This analysis produced limited meaningful alignments outside RND transporters. Expectedly, MmpL3 was most similar to other *Mtb* MmpL proteins. Conserved residues are located for the most part in TMS domains [Fig. S4]. Most striking is the conservation of charged residues in TMS-4, TMS-10 and TMS-12 of all MmpL proteins: D251, D640, D710 and R715 in MmpL3.[7,18,25,38] The location of these residues suggests that they may be the functional analogs of the AcrB D407, D408 (TMS-4) and K940, R971 (TMS-10) residues required for proton translocation and conformational changes.[10] R259 located in TMS-4 is also conserved [Fig. S4]. Also worth noting is the conservation among MmpL proteins of a proline residue in TMS-6 (P330 in MmpL3) [Fig. S4] and the presence of two additional, albeit non-conserved, prolines in TMS-7 of MmpL3 (P402 and P413). Proline residues in the TMS of various transporters have been previously implicated in functionally significant conformational transitions.[39-40]

To assess whether any of these conserved MmpL residues were important for the function of MmpL3, we mutated them by site-directed mutagenesis and analyzed the ability of the different MmpL3 mutants to rescue the viability of an *Msmg mmpL3* knock-out mutant (*MsmgΔmmpL3*), indicative of active TMM export. Inability to disrupt *mmpL3* in *Msmg* in the presence of some mutated copies of MmpL3 from *Mtb* indicates, on the contrary, that the activities of these mutated forms of the transporter are not sufficient to sustain growth. In addition to the MmpL3 variants mutated in the charged residues and proline residues

described above, the Cys-mutated ΔCys-MmpL3 variants used in our topology studies and an additional 20 Cys-mutated variants selected to probe the various cytoplasmic and periplasmic loops of the transporter [Fig. S3b] were tested for activity in *Msmg* (a total of 59 Cys-mutated variants tested). That all MmpL3 variants were produced in *Msmg* was verified by immunoblotting using rabbit polyclonal antibodies raised against the soluble C-terminal domain of MmpL3 [Fig. 5a]. Most mutants were produced at comparable if not greater levels than the control, ΔCys-MmpL3, with the exception of S288T, S288C, Q304C, D550C, S691C, whose expression levels were 40 to 60% less [Fig. 5a].

Of all the *mmpL3* mutants tested, seven failed to rescue the growth of *MsmgΔmmpL3* despite three independent attempts at 30 and 37°C: D251C; S288C; G543C; D640C; Y641C; D710C; R715C. Five of these mutants correspond to the conserved charged (or immediately adjacent) TMS-4, TMS-10 and TMS-12 residues D251, D640, Y641, D710 and R715 [Fig. 3b-c and Fig. S4] thought to be involved in proton translocation and conformational changes. In the MmpL3 model, all of these residues are co-localized in the core of the transmembrane domain and likely to be functionally linked by forming a putative "proton relay" site. The sixth inactive mutation, S288C, is located in TMS-5 and co-localizes in the MmpL3 model with the same putative "proton relay" site [Fig. 3a]. S288 is highly conserved among MmpL proteins [Fig. S4] and its functional significance is likely related to that of other residues at this site. Interestingly, a missense mutation changing S288 to a threonine was associated with high-level indolecarboxamide and adamantyl urea resistance in *Mtb*.[33] The fact that a S288T mutant was able to rescue the viability of *MsmgΔmmpL3* whereas the S288C mutant was not [Fig. 5] indicates that an oxygen to sulfur change at this position of MmpL3 dramatically reduces activity. In line with these observations, mutations in other residues located in the proposed proton relay site [G253 in TMS-4] or proximal to that site [the conserved R259 TMS-4 residue mentioned above and the MmpL-conserved T675 residue in TMS-11], while capable to rescuing the viability of *MsmgΔmmpL3*, significantly reduced MmpL3 activity based on growth on 7H11 agar and mycolic acid transfer to arabinogalactan [Fig. 5].

The seventh inactive mutant, G543C, is located on the modeled interface between PN and PC of the porter domain [Fig. S2]. G543 is also highly conserved among MmpL proteins [Fig. S4]. Interestingly, the Cys substitution of another highly conserved residue located in the same region, D550, also significantly reduced the activity of MmpL3 [Fig. 5b-c]. In the model, D550 lines the channel's entrance [Fig. S2]. Thus, both G543C and D550C are likely to affect the same functionally important interface between the two large periplasmic loops, possibly reducing the channel's activity.

Other mutations that significantly reduced MmpL3 activity included Q304 (periplasmic loop between TMS-5 and TMS-6) which points into the vestibule and lines the pore, and both P625 (periplasmic loop between TMS-9 and TMS-10) and S691 (periplasmic loop between TMS-11 and TMS-12; MmpL-conserved) which also line the pore [Fig. 3a]. The P330C, P402C and P413C mutants were functional and restored wild-type growth in *MsmgΔmmpL3* indicating that these Pro residues do not play a critical role in substrate export.

To finally determine whether mutations affecting the activity of MmpL3 had any impact on the susceptibility of *Msmg* to drugs affecting cell wall synthesis or other processes, our entire collection of *Msmg* strains expressing Cys-mutated ΔCys-MmpL3 variants was tested for susceptibility to penicillins, isoniazid, ciprofloxacin and rifampicin. While most of the mutants tested showed no significant differences in MICs relative to their control parent, the S288T, D550C and S691C mutants shown in Fig. 5 b-c displayed four- to eight-fold increased susceptibilities to penicillins and rifampicin [Table S2] suggestive of the increased permeability of their cell envelope to these drugs and/or of the hypersusceptibility of these mutants to drugs affecting cell wall biosynthetic processes. The same three mutants displayed, in contrast, parental susceptibility to isoniazid and ciprofloxacin [Table S2].

The C-terminal domain of MmpL3 is not essential for activity

The cytoplasmic C-terminal domain of MmpL3 was proposed to mediate the subcellular localization of MmpL3 at the poles and septa of dividing *Msmg* cells where the *de novo* biosynthesis of mycolic acids and peptidoglycan is thought to occur.[41] To determine whether the soluble C-terminal segment of MmpL3 from *Mtb* was required for growth, seven C-terminally truncated versions of MmpL3 terminating the protein at residues 915, 859, 777, 762, 750, 744 and 721 were cloned in the mycobacterial expression plasmid pMVGH1 and tested for their ability to rescue the growth of *Msmg*Δ*mmpL3*. All truncated versions of MmpL3 were functional and restored wild-type growth in the complemented mutants, with the exception of the shorter one interrupting the protein at residue 721 (located in TMS-12) which failed to express in *Msmg*. Thus, the C-terminal domain of MmpL3 is apparently not essential to the activity of the transporter or cell division/cell growth.

Chemical modification of cysteines identifies the periplasmic functional site of MmpL3

As a complementary approach to the functional assessment of the MmpL3 mutants in *Msmg*, we tested whether the replacement of amino acid residues by cysteines rendered MmpL3 susceptible to inhibition by thiol-reactive agents. To this end, *Msmg*Δ*mmpL3* strains expressing all of the functional Δ*Cys-mmpL3* mutants described above were tested for susceptibility to the sulfhydryl-reactive agents, ebselen and 2-sulfonatoethyl methanethiosulfonate (MTSES). While the treatment of *Msmg*Δ*mmpL3* cells expressing the parent ΔCys-MmpL3 protein with ebselen had no effect on growth at concentrations up to 40 μg/ml, the addition of 10 μg/ml ebselen to cells producing ΔCys-MmpL3 with Cys substitutions at positions Q40, Y235, and P625 reproducibly inhibited growth. Likewise, incubation with MTSES (512 μg/ml) inhibited the growth of cells producing ΔCys-MmpL3 variants with Cys substitutions at positions P625 and V694 (greater than 4-fold increase in susceptibility relative to the parent strain). The amino acid residues identified through this approach map to various periplasmic regions of MmpL3 (Q40 at the subunit interface in PN; Y235 between TMS-3 and TMS-4; P625 between TMS-9 and TMS-10; V694 between TMS-11 and TMS-12) [Fig. 3a], vicinal to the pore identified in CmpL1. That growth inhibition in these mutants was caused by the loss of activity of MmpL3 was verified by analyzing mycolic acid transfer to outer membrane lipids in the treated cells upon metabolic labeling with [1,2-^{14}C]acetic acid. In all cases, a build-up in TMM that accompanied a decrease in TDM formation was observed [Fig. S5]. That the proposed role of MmpL3 in heme-iron import contributes to growth defect is unlikely given the ability of the *Msmg*

recombinant strains used herein to produce siderophores and, thus, to use the ferric ion present in the different culture media.[23-24]

Collectively, our functional studies show that functionally important residues of MmpL3 are clustered into three sites: the central region of the transmembrane segments, the interface between the transmembrane and the porter domains vicinal to the pore structure, and the interface between the PN and PC loops of the porter domain that includes the channel feature. The transmembrane site is very extensive and, in addition to TMS-4 and TMS-10, also includes residues from TMS-12. It is unlikely that all of these residues contribute to proton translocation but they could also be essential for proton-driven conformational changes in the transporter. Alternatively, these residues line the large shared substrate-proton binding pocket. The interface between the transmembrane and the porter domain could be important for communicating conformational changes between the two domains.

TmaT acetylation is required for the export of TMM in mycobacteria

A recent study suggested that the acetylation of TMM by the *Cgl* acetyltransferase TmaT may be a prerequisite for the export of TMM in this species.[42] TMM acetylation would follow the transfer of mycolic acids onto trehalose by Pks13 [43] and, perhaps, serve as a signal for export by MmpL3 or another component of the mycolic acid translocation machinery. Whether acetylation is required for TMM export in mycobacteria was not known. To address this question, we generated a conditional *tmaT* (*MSMEG_0319*) knock-down of *Msmg* [Fig. 6a] and analyzed the effect of silencing this gene on bacterial growth and cell envelope biogenesis. MSMEG_0319 displays 41% identity (53% similarity) with the *Cgl* TmaT enzyme, and 74% identity (81% similarity) with *Mtb* TmaT (Rv0228) whose encoding gene was predicted to be essential based on saturation transposon mutagenesis.[44] Growth of *Msmg*Δ*tmaT*/pSETet-*tmaT* in the absence of ATc where the expression of *tmaT* is lost led to cell death clearly indicating that this gene is essential for growth [Fig. 6b]. An ATc concentration-dependent reduction in TDM synthesis and mycolic acid transfer onto cell wall arabinogalactan that accompanied an accumulation of TMM followed *tmaT* silencing [Fig. 6c]. These effects were not observed in the control strain (*Msmg*/pSETet-*tmaT*) [Fig. 6c] and are reminiscent of those caused by the silencing of *mmpL3*.[27] In conclusion, similar to the situation in *Cgl*, *tmaT* silencing impacts TMM export in mycobacteria. However, in contrast to the situation in *Cgl* where *tmaT* inactivation only partially inhibits trehalose dicorynomycolates formation and does not significantly affect the transfer of mycolates to arabinogalactan [42], *tmaT* silencing in *Msmg* had a much more drastic effect on the cells, abolishing both the transfer of mycolic acids onto cell wall arabinogalactan and TDM formation, and resulting in cell death. The fact that two CmpL transporters (CmpL1 and CmpL4) participate in the export of TMM in *Cgl* [4,11] - one of which may translocate non-acetylated TMM - while only MmpL3 carries out this function in *Msmg*, may account for the different impact of silencing *tmaT* in the two species.

Resistance to MmpL3 inhibitors localizes to the putative proton path of MmpL3

Several chemical scaffolds were reported to inhibit *Mtb* growth through the inhibition of MmpL3. Resistance mutations were specifically mapped to MmpL3 and, in some cases, the same mutations enabled resistance to different classes of inhibitors.[26-34] For example,

missense mutations changing S288 to a threonine were associated with high-level indolecarboxamide and adamantyl urea resistance in *Mtb*.[33] In the MmpL3 model, frequently encountered resistance mutations cluster in the middle of the transmembrane domain and spatially overlap with functional residues [Fig. 7]. Resistance mutation L189R maps to TMS-2, L215S to TMS-3, G253E to TMS-4, S288T to TMS-5, T311I to TMS-6, S591I to TMS-9, F644I/L to TMS-10, V684A/G to TMS-11, and A700T to TMS-12. In most cases, these mutations significantly change the size or the polarity of amino acid side chains and, therefore, are likely to impact the packing of the TMS helices including that of the molecular architecture of the functional residues. These results suggest that the inhibitors might target the proton relay site of MmpL3 and that the conformational changes at this site enable resistance. Continued transport activity in face of such conformational changes suggests plasticity in the substrate/proton translocation mechanism.

CONCLUSIONS

The studies described herein significantly advance our understanding of the structure and mechanism of translocation of HAE2 family proteins in *Corynebacteriaceae*. The negative staining electron microscopy map of CmpL1 validated the essential structural features of the *ab initio* sequence-derived model for CmpL1 and delineated a molecular architecture that resembles, in overall size and shape, the prototypical Gram-negative RND transporters. A number of critical functional residues were identified that map to the middle of the transmembrane helices of the transporter where resistance mutations to MmpL3 inhibitors have been reported. These regions of MmpL3 thus define areas of susceptibility to chemical inhibition that may further be exploited in the process of inhibitor screening and optimization. Importantly, the nature and location of the resistance mutations point to conformational changes as being the likely mechanism through which mutations may prevent inhibitors from accessing their binding site on MmpL3, and provide the first plausible explanation as to how the same mutation may confer resistance to multiple chemical scaffolds. More studies are in progress in our laboratories to validate the specific role of these functional residues and resistance mutations, and map the (Ac)TMM-binding site.

Another critical question that remains to be addressed is that of the extent of (Ac)TMM translocation mediated by MmpL3 and, in particular, whether this transporter captures its substrate from the periplasmic and/or the cytoplasmic face of the plasma membrane. Our results suggest a putative substrate/proton translocation path within the transporter implicating a periplasmic pore structure and spanning from the transmembrane to the periplasmic porter domain. The existence of a potential transmembrane transport tunnel linking the cytoplasm with the periplasm in MmpL proteins was also supported by molecular dynamical simulations from an *ab initio* modeled MmpL5 structure.[25] Such a pathway is consistent with what is known of the mechanism of translocation of HAE1 RND transporters that capture their substrates from both sides of the plasma membrane. Our observation that the last acylation steps of the substrates of MmpL10 (i.e., di- and penta-acyltrehaloses) occur on the periplasmic face of the plasma membrane,[14] suggest that MmpL proteins may be able to capture their substrates from the outer leaflet of the plasma membrane, and thus participate in the intermembrane transport of (glyco)lipids across the

periplasm, in addition to translocating them across the plasma membrane. If this is the case, however, CmpL1/MmpL3, similar to HAE1 RND efflux pumps, would have to function with other periplasmic adapters, OM proteins and, perhaps, inner membrane transporters to bring (Ac)TMM to the cell surface as their overall length (100Å of which an estimated 35Å extends in periplasmic space) is not compatible with a direct delivery of their substrates to the OM (the thickness of the mycobacterial/corynebacterial cell envelope is in the range of ~ 35-40 nm).[45-46] Studies on the export of sulfolipids,[47] phthiocerol dimycocerosates[16,48], glycopeptidolipids[49-50] and siderophores [13] in fact concur to support the existence of such additional transporters. Their definition and functional characterization represents an exciting field of study that awaits further investigations.

METHODS

Expression and purification of WT and mutated MmpL3 and CmpL1 proteins in Cgl - Cgl cmpL1

WT and the *Mtb* MmpL3 Cys-mutated variants used in topology determination were expressed in *Cgl* ATCC 13032 from the multicopy IPTG-inducible expression plasmid pAN6, in-frame with the eight amino acid sequence of StrepTag-II.[51] The C-terminally truncated and point-mutated *Mtb* MmpL3 genes used in functional and topology studies were generated using standard PCR and two-step PCR overlap methods, respectively. For functional studies, the MmpL3 mutants were expressed from the mycobacterial replicative plasmid, pMVGH1, under control of the *hsp60* promoter,[27] and analyzed for their ability to rescue the viability of an *Msmg mmpL3* knock-out mutant (*Msmg*Δ*mmpL3*), indicative of active TMM export. See Supplementary Methods in the Supporting Information for details.

Transmembrane topology mapping of MmpL3

Membrane fractions prepared from IPTG-induced *Cgl* LY108 cells [4] harboring pAN6 expression plasmids were treated with fluorescein-5-maleimide and the reaction was terminated by addition of DTT. MmpL3 Cys-mutated variants were then purified by anti-Strep affinity chromatography from the membrane fractions prior to separation by SDS-PAGE. The fluorescence was measured using StormTM (GE Healthcare) and protein amounts visualized by silver nitrate staining. The subcellular localization of the soluble loops and C-terminal domain of the *Msmg* MmpL3 protein (MSMEG_0250) expressed in *Msmg*, was further investigated by generating MmpL3-GFP fusions in the expression plasmids pJB(−) and JB(+) as described.[14] See Supporting Information for details.

Structural modeling

I-TASSER [52] was used to prepare a model for the 3D structure of CmpL1 based on its primary amino acid sequence and the trimeric quaternary structure of CmpL1 was next built using the AcrB structure (PDB ID: 3D9B) as detailed in the Supplementary Methods.

Construction of a MSMEG_0319 knock-down mutant of Msmg

A conditional knock-down of *Msmg* expressing *MSMEG_0319 (tmaT)* under control of an *anhydro*-tetracycline-inducible promoter from plasmid pSETetR was generated by homologous recombination as described.[27] See Supporting Information for details.

Supplementary Material

Refer to Web version on PubMed Central for supplementary material.

ACKNOWLEDGMENTS

This work was supported by a grant from the Potts Memorial Foundation (to MJ), the National Institutes of Health / National Institute of Allergy and Infectious Diseases grants AI116525 (to MJ) and AI092486 (to H.I.Z), and by GEPROM – FRSQ Intramural funding (to J.S, I.R., A.Y. and L.F.). The content is solely the responsibility of the authors and does not necessarily represent the official views of the NIH. We thank Dr. Michael Bott (Institut für Bio- und Geowissenschaften, Germany) for the pAN6 expression plasmid. The Facility for Electron Microscopy Research at McGill University (FEMR) provided access to electron microscopes. Proteomics analyses were performed by the Center for Advanced Proteomics Analyses at the Université de Montréal, a Node of the Canadian Genomic Innovation Network that is supported by the Canadian Government through Genome Canada.

REFERENCES

1. Tseng TT, Gratwick KS, Kollman J, Park D, Nies DH, Goffeau A, Saier MH Jr. The RND permease superfamily: an ancient, ubiquitous and diverse family that includes human disease and development proteins. J. Mol. Microbiol. Biotechnol. 1999; 1:107–125. [PubMed: 10941792]
2. Saier MH Jr. Paulsen IT. Phylogeny of multidrug transporters. Semin. Cell Dev. Biol. 2001; 12:205–213. [PubMed: 11428913]
3. Jain, M.; Chow, ED.; and Cox, JS. The MmpL protein family. In: Daffé, M.; Reyrat, J-M., editors. The Mycobacterial Cell Envelope. ASM Press; Washington, DC: 2008. p. 201-210.
4. Yang L, Lu S, Belardinelli J, Huc-Claustre E, Jones V, Jackson M, Zgurskaya HI. RND transporters protect Corynebacterium glutamicum from antibiotics by assembling the outer membrane. MicrobiologyOpen. 2014; 3:484–496. [PubMed: 24942069]
5. Li W, Upadhyay A, Fontes FL, North EJ, Wang Y, Crans DC, Grzegorzewicz AE, Jones V, Franzblau SG, Lee RE, Crick DC, Jackson M. Novel insights into the mechanism of inhibition of MmpL3, a target of multiple pharmacophores in *Mycobacterium tuberculosis*. Antimicrob. Agents Chemother. 2014; 58:6413–6423. [PubMed: 25136022]
6. Chim N, Torres R, Liu Y, Capri J, Batot G, Whitelegge JP, Goulding CW. The Structure and Interactions of Periplasmic Domains of Crucial MmpL Membrane Proteins from Mycobacterium tuberculosis. Chem. Biol. 2015; 22:1098–1107. [PubMed: 26278184]
7. Sandhu P, Akhter Y. The internal gene duplication and interrupted coding sequences in the MmpL genes of Mycobacterium tuberculosis: Towards understanding the multidrug transport in an evolutionary perspective. Int. J. Med. Microbiol. 2015; 305:413–423. [PubMed: 25841626]
8. Nikaido H. Structure and mechanism of RND-type multidrug efflux pumps. Adv. Enzymol. Relat. Areas Mol. Biol. 2011; 77:1–60. [PubMed: 21692366]
9. Ruggerone P, Murakami S, Pos KM, Vargiu AV. RND efflux pumps: structural information translated into function and inhibition mechanisms. Curr. Top. Med. Chem. 2013; 13:3079–3100. [PubMed: 24200360]
10. Eicher T, Seeger MA, Anselmi C, Zhou W, Brandstatter L, Verrey F, Diederichs K, Faraldo-Gomez JD, Pos KM. Coupling of remote alternating-access transport mechanisms for protons and substrates in the multidrug efflux pump AcrB. eLife. 2014; 3:e03145.
11. Varela C, Rittmann D, Singh A, Krumbach K, Bhatt K, Eggeling L, Besra GS, Bhatt A. MmpL genes are associated with mycolic acid metabolism in mycobacteria and corynebacteria. Chem. Biol. 2012; 19:498–506. [PubMed: 22520756]
12. Pacheco SA, Hsu FF, Powers KM, Purdy GE. MmpL11 protein transports mycolic acid-containing lipids to the mycobacterial cell wall and contributes to biofilm formation in Mycobacterium smegmatis. J. Biol. Chem. 2013; 288:24213–24222. [PubMed: 23836904]
13. Wells RM, Jones CM, Xi Z, Speer A, Danilchanka O, Doornbos KS, Sun P, Wu F, Tian C, Niederweis M. Discovery of a siderophore export system essential for virulence of *Mycobacterium tuberculosis*. PLoS Pathog. 2013; 9:e1003120. [PubMed: 23431276]

14. Belardinelli JM, Larrouy-Maumus G, Jones V, de Carvalho LP, McNeil MR, Jackson M. Biosynthesis and Translocation of Unsulfated Acyltrehaloses in Mycobacterium tuberculosis. J. Biol. Chem. 2014; 289:27952–27965. [PubMed: 25124040]

15. Burbaud S, Laval F, Lemassu A, Daffé M, Guilhot C, Chalut C. Trehalose Polyphleates Are Produced by a Glycolipid Biosynthetic Pathway Conserved across Phylogenetically Distant Mycobacteria. Cell Chem. Biol. 2016; 23:278–289. [PubMed: 27028886]

16. Camacho LR, Constant P, Raynaud C, Laneelle MA, Triccas JA, Gicquel B, Daffé M, Guilhot C. Analysis of the phthiocerol dimycocerosate locus of Mycobacterium tuberculosis. Evidence that this lipid is involved in the cell wall permeability barrier. J. Biol. Chem. 2001; 276:19845–19854. [PubMed: 11279114]

17. Rousseau C, Winter N, Pivert E, Bordat Y, Neyrolles O, Ave P, Huerre M, Gicquel B, Jackson M. Production of phthiocerol dimycocerosates protects *Mycobacterium tuberculosis* from the cidal activity of reactive nitrogen intermediates produced by macrophages and modulates the early immune response to infection. Cell. Microbiol. 2004; 6:277–287. [PubMed: 14764111]

18. Domenech P, Reed MB, Barry CE III. Contribution of the *Mycobacterium tuberculosis* MmpL protein family to virulence and drug resistance. Infect. Immun. 2005; 73:3492–3501. [PubMed: 15908378]

19. Milano A, Pasca MR, Provvedi R, Lucarelli AP, Manina G, Ribeiro AL, Manganelli R, Riccardi G. Azole resistance in Mycobacterium tuberculosis is mediated by the MmpS5-MmpL5 efflux system. Tuberculosis. 2009; 89:84–90. [PubMed: 18851927]

20. Hartkoorn RC, Uplekar S, Cole ST. Cross-resistance between clofazimine and bedaquiline through upregulation of MmpL5 in Mycobacterium tuberculosis. Antimicrob. Agents Chemother. 2014; 58:2979–2981. [PubMed: 24590481]

21. Andries K, Villellas C, Coeck N, Thys K, Gevers T, Vranckx L, Lounis N, de Jong BC, Koul A. Acquired resistance of Mycobacterium tuberculosis to bedaquiline. PLoS ONE. 2014; 9:e102135. [PubMed: 25010492]

22. Gilleron M, Stenger S, Mazorra Z, Wittke F, Mariotti S, Böhmer G, Prandi J, Mori L, Puzo G, De Libero G. Diacylated sulfoglycolipids are novel mycobacterial antigens stimulating CD1-restricted T cells during infection with *Mycobacterium tuberculosis*. J. Exp. Med. 2004; 199:649–659. [PubMed: 14981115]

23. Tullius MV, Harmston CA, Owens CP, Chim N, Morse RP, McMath LM, Iniguez A, Kimmey JM, Sawaya MR, Whitelegge JP, Horwitz MA, Goulding CW. Discovery and characterization of a unique mycobacterial heme acquisition system. Proc. Natl. Acad. Sci. U S A. 2011; 108:5051–5056. [PubMed: 21383189]

24. Owens CP, Chim N, Graves AB, Harmston CA, Iniguez A, Contreras H, Liptak MD, Goulding CW. The Mycobacterium tuberculosis secreted protein Rv0203 transfers heme to membrane proteins MmpL3 and MmpL11. J. Biol. Chem. 2013; 288:21714–21728. [PubMed: 23760277]

25. Sandhu P, Akhter Y. The drug binding sites and transport mechanism of the RND pumps from Mycobacterium tuberculosis: Insights from molecular dynamics simulations. Arch. Biochem. Biophys. 2016; 592:38–49. [PubMed: 26792538]

26. La Rosa V, Poce G, Canseco JO, Buroni S, Pasca MR, Biava M, Raju RM, Porretta GC, Alfonso S, Battilocchio C, Javid B, Sorrentino F, Ioerger TR, Sacchettini JC, Manetti F, Botta M, De Logu A, Rubin EJ, De Rossi E. MmpL3 Is the Cellular Target of the Antitubercular Pyrrole Derivative BM212. Antimicrob. Agents Chemother. 2012; 56:324–331. [PubMed: 22024828]

27. Grzegorzewicz AE, Pham H, Gundi VA, Scherman MS, North EJ, Hess T, Jones V, Gruppo V, Born SE, Korduláková J, Chavadi SS, Morisseau C, Lenaerts AJ, Lee RE, McNeil MR, Jackson M. Inhibition of mycolic acid transport across the *Mycobacterium tuberculosis* plasma membrane. Nat. Chem. Biol. 2012; 8:334–341. [PubMed: 22344175]

28. Tahlan K, Wilson R, Kastrinsky DB, Arora K, Nair V, Fischer E, Barnes SW, Walker JR, Alland D, Barry CE 3rd, Boshoff HI. SQ109 targets MmpL3, a membrane transporter of trehalose monomycolate involved in mycolic acid donation to the cell wall core of Mycobacterium tuberculosis. Antimicrob. Agents Chemother. 2012; 56:1797–1809. [PubMed: 22252828]

29. Stanley SA, Grant SS, Kawate T, Iwase N, Shimizu M, Wivagg C, Silvis M, Kazyanskaya E, Aquadro J, Golas A, Fitzgerald M, Dai H, Zhang L, Hung DT. Identification of novel inhibitors of

M. tuberculosis growth using whole cell based high-throughput screening. ACS Chem. Biol. 2012; 7:1377–1384. [PubMed: 22577943]

30. Poce G, Bates RH, Alfonso S, Cocozza M, Porretta GC, Ballell L, Rullas J, Ortega F, De Logu A, Agus E, La Rosa V, Pasca MR, De Rossi E, Wae B, Franzblau SG, Manetti F, Botta M, Biava M. Improved BM212 MmpL3 inhibitor analogue shows efficacy in acute murine model of tuberculosis infection. PLoS ONE. 2013; 8:e56980. [PubMed: 23437287]
31. Remuinan MJ, Perez-Herran E, Rullas J, Alemparte C, Martinez-Hoyos M, Dow DJ, Afari J, Mehta N, Esquivias J, Jimenez E, Ortega-Muro F, Fraile-Gabaldon MT, Spivey VL, Loman NJ, Pallen MJ, Constantinidou C, Minick DJ, Cacho M, Rebollo-Lopez MJ, Gonzalez C, Sousa V, Angulo-Barturen I, Mendoza-Losana A, Barros D, Besra GS, Ballell L, Cammack N. Tetrahydropyrazolo[1,5-a]Pyrimidine-3-Carboxamide and N-Benzyl-6',7'-Dihydrospiro[Piperidine-4,4'-Thieno[3,2-c]Pyran] Analogues with Bactericidal Efficacy against Mycobacterium tuberculosis Targeting MmpL3. PLoS ONE. 2013; 8:e60933. [PubMed: 23613759]
32. Ioerger TR, O'Malley T, Liao R, Guinn KM, Hickey MJ, Mohaideen N, Murphy KC, Boshoff HI, Mizrahi V, Rubin EJ, Sassetti CM, Barry CE 3rd, Sherman DR, Parish T, Sacchettini JC. Identification of New Drug Targets and Resistance Mechanisms in Mycobacterium tuberculosis. PLoS ONE. 2013; 8:e75245. [PubMed: 24086479]
33. Lun S, Guo H, Onajole OK, Pieroni M, Gunosewoyo H, Chen G, Tipparaju SK, Ammerman NC, Kozikowski AP, Bishai WR. Indoleamides are active against drug-resistant Mycobacterium tuberculosis. Nat. Commun. 2013; 4:2907. [PubMed: 24352433]
34. Rao SP, Lakshminarayana SB, Kondreddi RR, Herve M, Camacho LR, Bifani P, Kalapala SK, Jiricek J, Ma NL, Tan BH, Ng SH, Nanjundappa M, Ravindran S, Seah PG, Thayalan P, Lim SH, Lee BH, Goh A, Barnes WS, Chen Z, Gagaring K, Chatterjee AK, Pethe K, Kuhen K, Walker J, Feng G, Babu S, Zhang L, Blasco F, Beer D, Weaver M, Dartois V, Glynne R, Dick T, Smith PW, Diagana TT, Manjunatha UH. Indolcarboxamide is a preclinical candidate for treating multidrug-resistant tuberculosis. Sci. Transl. Med. 2013; 5:214ra168.
35. Tantry SJ, Degiacomi G, Sharma S, Jena LK, Narayan A, Guptha S, Shanbhag G, Menasinakai S, Mallya M, Awasthy D, Balakrishnan G, Kaur P, Bhattacharjee D, Narayan C, Reddy J, Naveen Kumar CN, Shandil R, Boldrin F, Ventura M, Manganelli R, Hartkoorn RC, Cole ST, Panda M, Markad SD, Ramachandran V, Ghorpade SR, Dinesh N. Whole cell screen based identification of spiropiperidines with potent antitubercular properties. Bioorg. Med. Chem. Lett. 2015; 25:3234–3245. [PubMed: 26087937]
36. Tsukazaki T, Mori H, Echizen Y, Ishitani R, Fukai S, Tanaka T, Perederina A, Vassylyev DG, Kohno T, Maturana AD, Ito K, Nureki O. Structure and function of a membrane component SecDF that enhances protein export. Nature. 2011; 474:235–238. [PubMed: 21562494]
37. Long JC, Wang S, Vik SB. Membrane topology of subunit a of the F1F0 ATP synthase as determined by labeling of unique cysteine residues. J. Biol. Chem. 1998; 273:16235–16240. [PubMed: 9632682]
38. Bernut A, Viljoen A, Dupont C, Sapriel G, Blaise M, Bouchier C, Brosch R, de Chastellier C, Herrmann JL, Kremer L. Insights into the smooth-to-rough transitioning in Mycobacterium bolletii unravels a functional Tyr residue conserved in all mycobacterial MmpL family members. Mol. Microbiol. 2016; 99:866–883. [PubMed: 26585558]
39. Ni Z, Bikadi Z, Shuster DL, Zhao C, Rosenberg MF, Mao Q. Identification of proline residues in or near the transmembrane helices of the human breast cancer resistance protein (BCRP/ABCG2) that are important for transport activity and substrate specificity. Biochemistry. 2011; 50:8057–8066. [PubMed: 21854076]
40. Babot M, Blancard C, Pelosi L, Lauquin GJ, Trezeguet V. The transmembrane prolines of the mitochondrial ADP/ATP carrier are involved in nucleotide binding and transport and its biogenesis. J. Biol. Chem. 2012; 287:10368–10378. [PubMed: 22334686]
41. Carel C, Nukdee K, Cantaloube S, Bonne M, Diagne CT, Laval F, Daffé M, Zerbib D. Mycobacterium tuberculosis proteins involved in mycolic acid synthesis and transport localize dynamically to the old growing pole and septum. PLoS ONE. 2014; 9:e97148. [PubMed: 24817274]

42. Yamaryo-Botte Y, Rainczuk AK, Lea-Smith DJ, Brammananth R, van der Peet PL, Meikle P, Ralton JE, Rupasinghe TW, Williams SJ, Coppel RL, Crellin PK, McConville MJ. Acetylation of trehalose mycolates is required for efficient MmpL-mediated membrane transport in Corynebacterineae. ACS Chem. Biol. 2015; 10:734–746. [PubMed: 25427102]

43. Gavalda S, Bardou F, Laval F, Bon C, Malaga W, Chalut C, Guilhot C, Mourey L, Daffé M, Quémard A. The polyketide synthase Pks13 catalyzes a novel mechanism of lipid transfer in mycobacteria. Chem. Biol. 2014; 21:1660–1669. [PubMed: 25467124]

44. Griffin JE, Gawronski JD, Dejesus MA, Ioerger TR, Akerley BJ, Sassetti CM. High-resolution phenotypic profiling defines genes essential for mycobacterial growth and cholesterol catabolism. PLoS Pathog. 2011; 7:e1002251. [PubMed: 21980284]

45. Hoffmann C, Leis A, Niederweis M, Plitzko JM, Engelhardt H. Disclosure of the mycobacterial outer membrane: cryo-electron tomography and vitreous sections reveal the lipid bilayer structure. Proc. Natl. Acad. Sci. USA. 2008; 105:3963–3967. [PubMed: 18316738]

46. Zuber B, Chami M, Houssin C, Dubochet J, Griffiths G, Daffé M. Direct visualization of the outer membrane of mycobacteria and corynebacteria in their native state. J. Bacteriol. 2008; 190:5672–5680. [PubMed: 18567661]

47. Seeliger JC, Holsclaw CM, Schelle MW, Botyanszki Z, Gilmore SA, Tully SE, Niederweis M, Cravatt BF, Leary JA, Bertozzi CR. Elucidation and chemical modulation of sulfolipid-1 biosynthesis in Mycobacterium tuberculosis. J. Biol. Chem. 2012; 287:7990–8000. [PubMed: 22194604]

48. Sulzenbacher G, Canaan S, Bordat Y, Neyrolles O, Stadthagen G, Roig-Zamboni V, Rauzier J, Maurin D, Laval F, Daffé M, Cambillau C, Gicquel B, Bourne Y, Jackson M. LppX is a lipoprotein required for the translocation of phthiocerol dimycocerosates to the surface of Mycobacterium tuberculosis. EMBO J. 2006; 25:1436–1444. [PubMed: 16541102]

49. Sonden B, Kocincova D, Deshayes C, Euphrasie D, Rhayat L, Laval F, Frehel C, Daffé M, Etienne G, Reyrat J-M. Gap, a mycobacterial specific integral membrane protein, is required for glycolipid transport to the cell surface. Mol. Microbiol. 2005; 58:426–440. [PubMed: 16194230]

50. Deshayes C, Bach H, Euphrasie D, Attarian R, Coureuil M, Sougakoff W, Laval F, Av-Gay Y, Daffé M, Etienne G, Reyrat JM. MmpS4 promotes glycopeptidolipids biosynthesis and export in *Mycobacterium smegmatis*. Mol. Microbiol. 2010; 78:989–1003. [PubMed: 21062372]

51. Frunzke J, Engels V, Hasenbein S, Gatgens C, Bott M. Co-ordinated regulation of gluconate catabolism and glucose uptake in Corynebacterium glutamicum by two functionally equivalent transcriptional regulators, GntR1 and GntR2. Mol. Microbiol. 2008; 67:305–322. [PubMed: 18047570]

52. Yang J, Yan R, Roy A, Xu D, Poisson J, Zhang Y. The I-TASSER Suite: protein structure and function prediction. Nat. Methods. 2015; 12:7–8. [PubMed: 25549265]

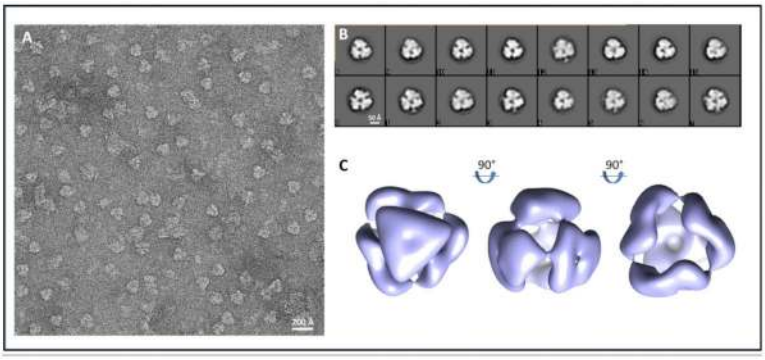

Figure 1. Negative staining electron microscopy of CmpL1

(**a**) Field of view showing purified CmpL1 particles negatively stained with uranyl formate. (**b**) Representative two-dimensional class averages of particles at different orientations. (**c**) *Ab initio* 3D reconstruction of CmpL1 contoured at high relative density to emphasize structural features.

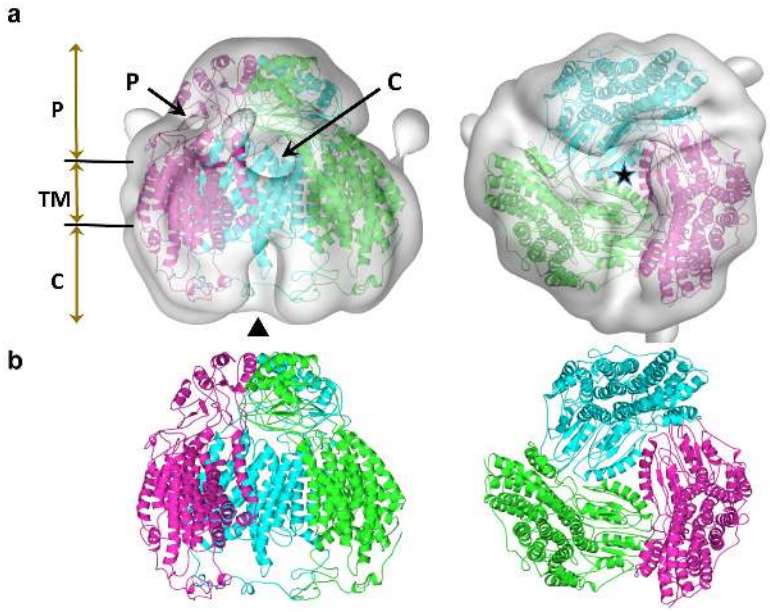

Figure 2. Superposition of the refined CmpL1 modeled structure onto the 3D negative staining EM maps

CmpL1 subunits are colored cyan, green and red to render them distinguishable. From left to right, the images in panels (**a**) and (**b**) are shown rotated by 90° relative to horizontal plane with view either parallel or perpendicular to the 3-fold rotation axis.

(**a**) Reconstructed CmpL1 3D EM map with surface contoured at a relative level = 3, with refined CmpL1 structure depicted by its secondary structure elements. The EM map is shown as semi-transparent. The vestibule region in the CmpL1 trimer is marked by a star in the right panel (**a**), while **P** designates the pore structure located between the TM helices and the periplasmic domain of a subunit; ▲ locates the subunit interface region which forms a crevasse on the inner leaflet side and leads into the vestibule, and **C** designates a channel leading from the outer leaflet into the vestibule. The vertical lettering **P**, **TM**, and **C** on the left hand side of the upper initial figure corresponds to the periplasmic region of CmpL1, its transmembrane region and the cytoplasmic accessible side, respectively.

(**b**) The corresponding images of the refined CmpL1 structure used to fit the EM map.

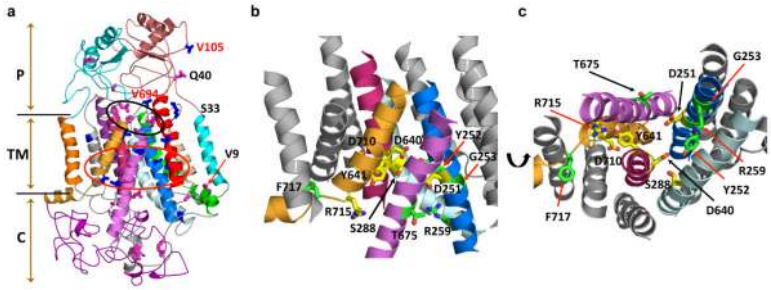

Figure 3. Structural model for the MmpL3 transporter

(**a**) Model showing the secondary structure elements of the MmpL3 subunit derived by threading the MmpL3 amino acid sequence onto the CmpL1 structural template using I-TASSER. Residue side chains whose mutations to Cys residues were accessible to the fluorescein-5-maleimide (FM) probe are shown in pink, while inaccessible residues are shown in blue. The letters **TM**, **P** and **C** on the left hand side refer to the transmembrane region, periplasmic and cytoplasmic accessible side of MmpL3, respectively. The TM helices are color coded to improve visibility. From left to right TMS-7 (orange), TMS-9 (gray), TMS-8 (violet purple), TMS-10 (pink), TMS-12 (bright orange), TMS-11 (violet), TMS-5 (pale cyan), TMS-4 (marine), TMS-6 (green), TMS-2 (red), TMS-3 (wheat) and TMS-1 (cyan). The periplasmic domains PN (34-173) and PC (417-551) are colored deep salmon and cyan, respectively. The C-terminal region (729-944) is colored purple. Residues lettered red, namely V105 and V694, situated in the periplasmic region of MmpL3 and whose Cys mutations were inaccessible to FM were not solvent accessible in the MmpL3 model which may preclude their accessibility to the probe. The pore region is circled in black and encompasses probe accessible Cys mutant residues Y235, Q304, L615, P625, and S691.

(**b**) The region, circled in red in (**a**), encompasses residues whose Cys mutations resulted in significant reduction in transport activity, shown in green, and residues whose Cys mutation abolished transport activity, colored yellow.

(**c**) The image is the same as in (**b**) with view rotated 90° and looking down from the cytoplasmic side. In (**b**) and (**c**), only the helices which contributed the side chains affecting transport activity are colored: TMS-10 (pink), TMS-12 (bright orange), TMS-5 (pale cyan), TMS-4 (marine); TMS-11 (violet).

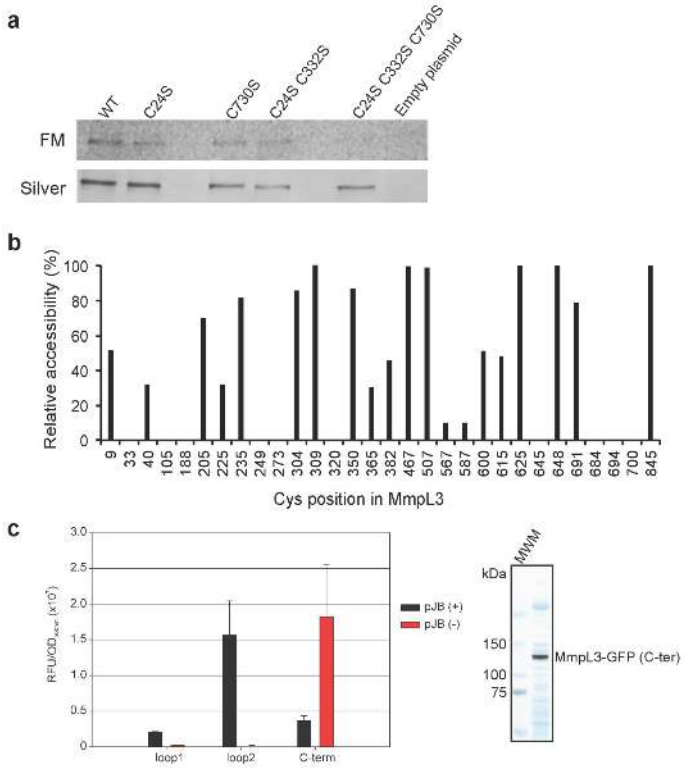

Figure 4. Transmembrane topology of MmpL3

(**a**) FM labeling of *Cgl* LY108 cells harboring either an empty pAN6 plasmid, or expressing WT *Mtb* MmpL3 (WT) or variants of this protein in which one or more of the endogenous Cys residues (C24, C332 and C730) were mutated to serine.

(b) Accessibility of the Cys-substituted ΔCys-MmpL3 variants to modification with the thiol-reactive fluorescent probe, FM. *Cgl* cells harboring expression plasmids encoding the indicated ΔCys-MmpL3 variants were induced with IPTG and membrane fractions were isolated as described in the Supplementary Methods. Upon labeling with FM, the reactions were quenched with DTT, membrane proteins solubilized with detergent and the ΔCys-MmpL3 variants were purified by affinity chromatography. Fractions containing the eluted proteins were separated by 8% SDS-PAGE and fluorescence quantified using a Storm Imager and ImageJ software. The ΔCys-MmpL3 variant harboring the A845C substitution in the cytoplasmic C-terminal domain was highly accessible to FM modification and was used as a positive control in all experiments. The fluorescence intensity of each of the ΔCys-MmpL3 variants was expressed relative to the fluorescence intensity of the ΔCys-MmpL3 mutant harboring the A845C substitution arbitrarily set to 100%.

(**c**) Subcellular localization of the two large soluble loops and C-terminal end of MmpL3 in *M. smegmatis* (*Msmg*). Inframe 3'fusions between residues 171 (loop 1), 563 (loop 2) or 1013 (C-term) (of MmpL3 and GFP were generated in pJB(−) and JB(+) as described in the Supplementary Methods section. Left panel: Fluorescence intensities were normalized to the OD_{600} of the cultures. The differences in fluorescence intensities between *Msmg* pJB(−)/(+)*mmpL3*-171, pJB(−)/(+)*mmpL3*-563 and pJB(−)/(+)*mmpL3*-1013 transformants were statistically significant per Student's *t*-test ($p < 0.05$) and confirmed the periplasmic location of the two large soluble loops of MmpL3 and the cytosolic location of its C-terminal

domain. Right panel: SDS-PAGE analysis of the C-ter GFP-tagged MmpL3 protein (fused to GFP at residue 1013). Fluorescent MmpL3-GFP was detected by PhosphorImager. A fluorescent band is visible at the expected size (~ 140 KDa) by superimposing the PhosphorImager image with the Coomassie blue-stained gel.

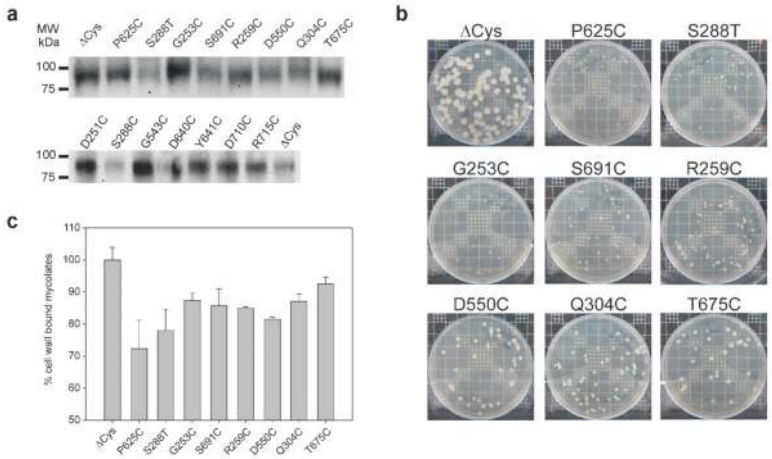

Figure 5. Functional analysis of MmpL3 mutants in *M. smegmatis*

(**a**) Western blot analysis of fifteen MmpL3 mutants expressed in *M. smegmatis* (*Msmg*). The top gel shows the Cys-mutated ΔCys-MmpL3 variants capable of rescuing the viability of *Msmg*Δ*mmpL3* albeit with a reduced transport activity. The lower gel carries the MmpL3 variants whose transport activity is either abolished or reduced below the level required to rescue the viability of the knock-out mutant. Total protein extracts were prepared from *Msmg* expressing ΔCys-MmpL3 (ΔCys) or the Cys-mutated ΔCys-MmpL3 variants [D251C; G253C; R259C; S288C; S288T; Q304C; G543C; D550C; P625C; D640C; Y641C; T675C; S691C; D710C; and R715C] from pMVGH1; 30 μg of total protein extracts from each strain were separated by SDS-PAGE and analyzed by immunoblot using a rabbit polyclonal antibody directed to the C-terminal soluble domain of the MmpL3 protein from *Mtb*. This antibody does not react with the endogenous MmpL3 protein from WT *Msmg* mc^2155 (not shown).

(**b**) Growth of *Msmg*Δ*mmpL3* expressing either the parent ΔCys-MmpL3 or the eight Cys-mutated ΔCys-MmpL3 variants shown in (**a**) (top gel) on 7H11-ADC agar after six days of incubation at 37°C.

(**c**) MmpL3 activity of the rescued *Msmg* mutants shown in (**b**). The [1,2-^{14}C-acetate]-derived cell wall-bound mycolic acids prepared from the same biomass of each of the strains were quantified by scintillation counting. Reduced MmpL3 activity results in a decrease in mycolic acid transfer to arabinogalactan. Shown are the means and standard deviations of two independent metabolic labeling experiments. Results are expressed as percentages of [^{14}C]-labeled cell wall-bound mycolic acids in the mutants relative to the ΔCys-MmpL3 parent strain (arbitrarily set to 100%).

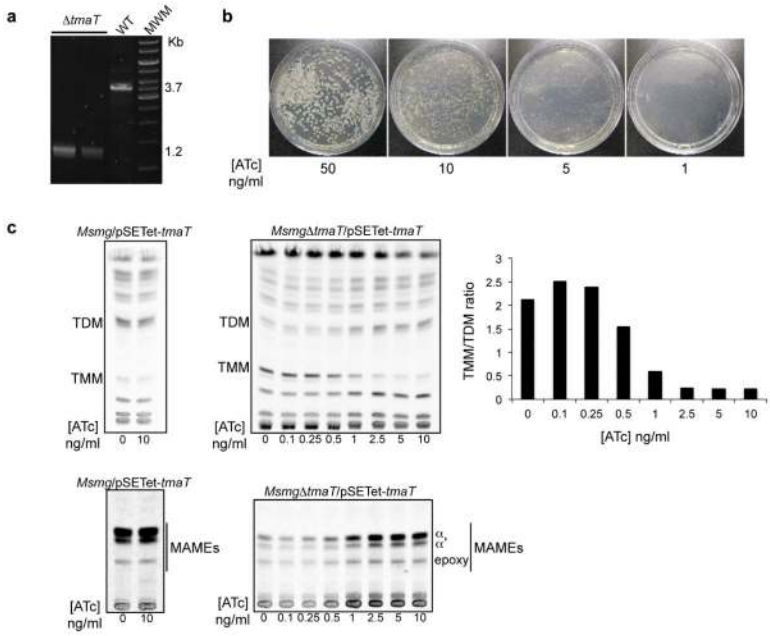

Figure 6. Effect of silencing *tmaT* on *Msmg* growth and mycolic acid export

(**a**) Allelic replacement at the *tmaT* locus of *Msmg* rescued with WT *tmaT* expressed from pSETetR under control of an ATc-inducible (TET-ON) promoter was confirmed by PCR in two independent clones. PCR fragments were digested with EcoRI. The WT 3.7-Kb amplification signal is replaced by three ~ 1.2 Kb fragments in the mutants due to the replacement of the *tmaT* ORF by a 1.2 kb- kanamycin resistance cassette (harboring two EcoRI restriction sites).

(**b**) Growth of the *Msmg*Δ*tmaT*/pSETet-*tmaT* conditional knock-down strain on 7H11-ADC plates in the presence of different concentrations of ATc. TmaT is essential for growth in *Msmg*.

(c) Effect of silencing *tmaT* on mycolic acid export. Total [1,2-^{14}C-acetate]-derived lipids and cell wall-bound mycolates from the conditional knock-down (*Msmg*Δ*tmaT*/pSETet-*tmaT*) and control strain (*Msmg*/pSETet-*tmaT*) grown in the presence of different concentrations of ATc were analyzed by TLC in the solvent systems ($CHCl_3$:CH_3OH:H_2O; 20:4:0.5, by vol.) for total lipids, and (*n*-hexane:ethyl acetate; 95:5, by vol.) for mycolic acid methyl esters (MAMEs). For lipid analysis, the same total counts (10,000 dpm) for each sample was loaded per lane. The amount of radioactivity incorporated in TMM and TDM in the conditional knock-down was semi-quantified using a PhosphoImager and the results, expressed as TMM/TDM ratios, are presented alongside the autoradiogram. For cell wall-bound mycolic acid analysis, samples were loaded volume to volume. ATc concentration does not impact the transfer of mycolic acids onto cell wall arabinogalactan or TDM in the control strain, *Msmg*/pSETet-*tmaT*.

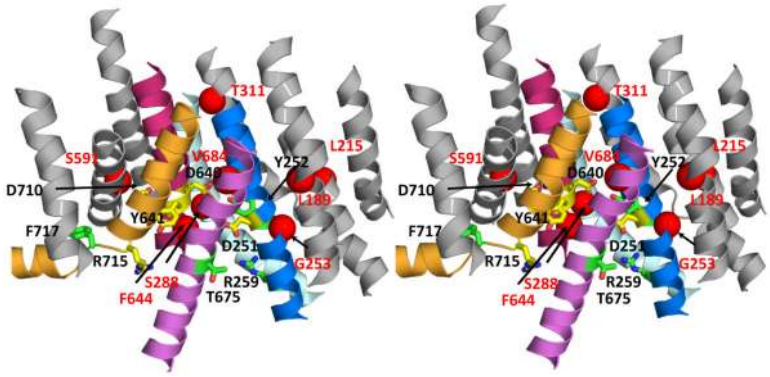

Figure 7. Stereo image showing resistance mutations in MmpL3 superimposed on the MmpL3 model displaying the functional mutations located in the transmembrane region as shown in Fig. 3b

The position of frequently encountered resistance mutations to one or more MmpL3 inhibitors are shown as red spheres centered on the Cα atom of the native MmpL3 residue. These residues map to transmembrane helices. Residues whose mutations to Cys resulted in significant reduction in transport activity are shown in green and those whose Cys mutation abolished transport activity are colored yellow.

Table 1

Real-space refinement of CmpL1 model against the EM envelope.

Metric	
Resolution of EM map	16-20Å
Map CC [a]	0.742
rmsd (bonds):	0.01Å
rmsd (angles):	2.10°
All-atom clashscore [b]	34.4
Ramachandran plot:	
outliers:	1.17 %
allowed:	24.81 %
favored:	74.03 %
Rotamer outliers:	2.58 %
C-beta deviations:	9

[a] Correlation coefficient between map density and atomic coordinates of model

[b] calculated as 1000 * (number of bad overlaps) / (number of atoms)